Solar Phys (2008) 253: 199–214
DOI 10.1007/s11207-008-9234-4

Particle Interactions with Single or Multiple 3D Solar Reconnecting Current Sheets

A. Anastasiadis · C. Gontikakis · C. Efthymiopoulos

Received: 29 November 2007 / Accepted: 12 June 2008 / Published online: 8 August 2008

Abstract The acceleration of charged particles (electrons and protons) in flaring solar active regions is analyzed using numerical experiments. The acceleration is modeled as a stochastic process taking place by the interaction of the particles with local magnetic reconnection sites via multiple steps. Two types of local reconnecting topologies are studied: the Harris-type and the X-point. A formula for the maximum kinetic energy gain in a Harris-type current sheet, found in a previous work of ours, fits well the numerical data for a single step of the process. A generalization is then given approximating the kinetic energy gain through an X-point. In the case of the multiple step process, in both topologies the kinetic energy distribution of the particles is found to acquire a practically invariant form after a small number of steps. This tendency is interpreted theoretically. Other characteristics of the acceleration process are given, such as the mean acceleration time and the pitch angle distributions of the particles.

Keywords Flares, energetic particles, acceleration · Magnetic fields

Radio Physics and the Flare-CME Relationship
Guest Editors: Karl-Ludwig Klein and Silja Pohjolainen.

A. Anastasiadis (✉)
National Observatory of Athens, Institute for Space Applications and Remote Sensing, 15236 Penteli, Greece
e-mail: anastasi@space.noa.gr

C. Gontikakis · C. Efthymiopoulos
Academy of Athens, Research Center of Astronomy and Applied Mathematics, Soranou Efessiou 4, 11527 Athens, Greece

C. Gontikakis
e-mail: cgontik@academyofathens.gr

C. Efthymiopoulos
e-mail: cefthim@academyofathens.gr

1. Introduction

The study of the energetic particle acceleration process during solar flares still remains an open and challenging problem for solar physics. Solar flares are the manifestation of the energy release process in the solar corona and atmosphere. It is well established that during this energy release process the free magnetic energy is converted, through magnetic reconnection, into heating, bulk motion of the flaring plasma and particle acceleration.

In the framework of the theory of magnetic reconnection during solar flares, a number of works in the literature have addressed the problem of particle acceleration. Several authors studied a steady state magnetic field topology, with an induced homogeneous electric field, using analytical methods or numerical integration of test particles. The magnetic field topology is either an X-point, with or without the presence of a longitudinal component (Bulanov, 1980; Burkhart, Drake, and Chen, 1990; Deeg, Borovsky, and Duric, 1991; Bruhwiler and Zweibel, 1992; Moses, Finn, and Ling, 1993; Vekstein and Browning, 1997; Mori, Sakai, and Zhao, 1998; Browning and Vekstein, 2001; Zharkova and Gordovskyy, 2005; Hannah and Fletcher, 2006), or a reconnecting current sheet (RCS) (Martens, 1988; Martens and Young, 1990; Litvinenko, 1996; Zharkova and Gordovskyy, 2004). The purpose has been to study the final kinetic energy distribution of accelerated particles, the condition of adiabaticity of their orbits and the level of charge separation at the ejection points. More realistic steady X-point topologies were derived using the MHD equations (Craig and Litvinenko, 2002; Heerikhuisen, Litvinenko, and Craig, 2002) and, in some cases, three-dimensional reconnection topologies (Dalla and Browning, 2005) in order to study trajectories of the particles.

In order to model the burst effects, many authors have incorporated a time dependent electric field in X-points (Hamilton *et al.*, 2003, 2005; Fletcher and Petkaki, 1997; Petkaki and MacKinnon, 2007, 1997) or adopted a numerical code as Tajima *et al.* (1987). Wood and Neukirch (2005) modeled an X-point with a nonhomogeneous electric field that was stronger at its center. Finally, Kliem (1994) used O-point and X-point combinations to study the effect of the fragmentation of RCSs on the acceleration of particles. On the other hand, several studies (*e.g.*, Benz *et al.*, 1994; Saint-Hilaire and Benz, 2002) show that more than 40% of the energy released in solar flares is deposited to high energetic particles, indicating the close relation between the particle acceleration process and the way (and amount) of the energy released in these highly energetic events. Despite this, a very common approach to build acceleration models (see Miller *et al.*, 1997; Anastasiadis, 2002 for reviews) is to consider that the different processes (*i.e.*, energy release, acceleration, transport and radiation) are decoupled. The main reason for such a consideration is the very different temporal and spatial scales on which the different processes evolve. Notwithstanding this difference, it should be remembered that all the processes are interwoven in a way that it is necessary to develop *global models* for solar flares, *i.e.*, models taking into account the interplay between the individual processes.

Parker (1988) first proposed that the free magnetic energy could be released in the solar corona through *multiple dissipation sites*. This assumption implies essentially the fragmentation of the energy release in both space and time during solar flares. A number of observations, related to either solar flare parameters (*e.g.*, Dennis, 1985; Benz, 1985; Crosby, Aschwanden, and Dennis, 1993; Crosby *et al.*, 1998; Aschwanden *et al.*, 1995, 2000) or emission processes in the solar corona (*e.g.*, Mercier and Trottet, 1997; Krucker and Benz, 1998), have been interpreted on the basis of such a scenario. In view of such an interpretation, several models of particle acceleration that incorporate concepts from the general theory of dynamical systems, such as the *complexity* of the energy release process

have been developed. For example, Anastasiadis and Vlahos (1991, 1994) assumed the presence of multiple shock waves acting on the particles. Such shocks have the form of small-scale, short-lived magnetic discontinuities inside a flaring active region. Another possibility is the acceleration of particles by multiple DC electric fields (Anastasiadis, Vlahos, and Georgoulis, 1997; Anastasiadis *et al.*, 2004; Vlahos, Isliker, and Lepreti, 2004; Dauphin, Vilmer, and Anastasiadis, 2007). Such fields are associated with the variety of dissipation sites inside an active region. A simulation of the energy release process can then be made using a cellular automaton (CA), the dynamical substrate of which assumes that the active region evolves according to the dynamical laws of a system being on the status of 'self-organizing criticality' (see Isliker, Anastasiadis, and Vlahos, 2001 for details on CA models for solar flares).

In the solar corona, large-scale and long lasting current sheets, in which a large number of particles could be accelerated, are unlikely to be present. Recent MHD simulations show that large current sheets are not stable for a long time and are quickly fragmented (Onofri, Isliker, and Vlahos, 2006). Furthermore, Hughes *et al.* (2003) have shown that solar flares can be considered as cascades of reconnecting small-scale magnetic loops inside an overall simple large magnetic field topology. In other words, the large-scale magnetic field topology probably determines the location of the magnetic energy release regions only on the scale of the active region. In addition, the complex magnetic environment of an active region together with the turbulent photospheric motions should be taken into account, since these external factors drive the system continuously by adding new stresses to the existing large-scale topologies. In particular, such a type of driving leads necessarily to the formation of multiple (RCS) configurations.

In the present work, we consider the above description as the basis for constructing numerical simulations of the acceleration of particles (electrons and protons) within multiple 3D current sheets developing in an active region. Our basic model is a sequence of encounter events of a population of particles with local current sheets with physical parameters changing stochastically. In order to understand the outcome of such a process, it is important to study first just one step of the process, namely the interaction of the particles with just one RCS. This was the basic motivation behind two recent papers of ours (Efthymiopoulos, Gontikakis, and Anastasiadis, 2005; Gontikakis, Efthymiopoulos, and Anastasiadis, 2006) in which we explored the particle dynamics and acceleration in a single Harris-type RCS configuration using numerical and analytical means. A basic outcome of our study is an analytical formula yielding the maximum possible kinetic energy gain of the particles passing through the RCS as a function of their initial kinetic energy and of the physical parameters of the current sheet. Our formula generalizes previous formulae given by Speiser (1965) and Litvinenko (1996), containing the latter as asymptotic limits. In the present paper we further generalize this formula to an approximate formula valid for single X-point topologies. Following the evaluation of this one-step process, we then pass to model the acceleration of particles inside a complex flaring active region as a stochastic process. In this we repeat the methodology used in Gontikakis, Anastasiadis, and Efthymiopoulos (2007) for Harris-type RCSs, and we provide a further theoretical analysis of the results obtained therein.

In summary, the simulations are done as follows: particles are initially interacting with a single RCS. This changes their kinetic energy distribution. After this interaction, the particles are considered to perform a free flight following the magnetic field lines until they reach another RCS present in the active region. This process is in principle repeated *ad infinitum*. Nevertheless, one finds that the kinetic energy distribution tends to acquire a limiting form following a few such steps, after which no appreciable change is seen in the distribution. This fact was observed in our previous study and we here provide a theoretical explanation

for it. Furthermore, we expand our study by considering also multiple encounters of the particles with local X-point reconnecting magnetic field configurations. In this we find again the tendency of the kinetic energy distribution to reach a limiting form. We thus conclude that this phenomenon is probably generic, *i.e.*, independent of the details of the reconnection topology.

In the next section (Section 2) we outline the basic characteristics of our numerical set up. In Section 3 the interaction of particles with a single RCS is studied, followed by our results for the multiple encounters (Section 4). Section 5 summarizes our results.

2. The Numerical Set-up

We assume two types of magnetic field reconnecting topologies. The first type is the Harris-type model of Litvinenko and Somov (1993) that represents one local current sheet within an active region. The magnetic and electric fields inside one sheet of half-thickness a are given in Equation (1):

$$\begin{aligned} E &= (0, 0, E), \\ B &= (-\mathrm{y}/a, \xi_\perp, \xi_\parallel) B_0 \quad \text{for } |\mathrm{y}| \le a. \end{aligned} \tag{1}$$

The edges of the current sheet are at $\mathrm{y} = \pm a$. The magnetic field is normalized in units of B_0, the value of the main reconnecting component at the edges. The magnetic field has two components, parallel and perpendicular to the current sheet plane, called the 'longitudinal' ($\xi_\parallel$) and 'transverse' ($\xi_\perp$) components, respectively. The second type is an X-point topology defined by the following equations:

$$\begin{aligned} E &= (0, 0, E), \\ B &= \big(-\mathrm{y}/a, -(\mathrm{x}/a)\xi_\perp, \xi_\parallel\big) B_0 \quad \text{for } |\mathrm{y}| \le a. \end{aligned} \tag{2}$$

Note that a Harris-type configuration is a simplified model for, say, the left domain of an X-point configuration far from the $\mathrm{x} = \mathrm{y} = 0$ point.

In Efthymiopoulos, Gontikakis, and Anastasiadis (2005), we studied the dynamics of the particles in a Harris-type RCS using the Hamiltonian equations of motions. We found that, using the symmetry of the problem, the initial 3-degrees of freedom Hamiltonian can be reduced to a two degrees of freedom Hamiltonian of the form:

$$H = \frac{1}{2} p_y^2 + \frac{1}{2}\left(c_4 + \frac{1}{2} y^2\right)^2 + \frac{1}{2}(I_2 - \xi_\perp z + \xi_\parallel y)^2 - \epsilon z, \tag{3}$$

with $\epsilon = Em/(aB_0^2 e)$ being the normalized electric field (m and e are the particle's mass and charge) and $x = \mathrm{x}/a$, $y = \mathrm{y}/a$, $z = \mathrm{z}/a$ are the normalized space coordinates. The time coordinate, implicit in Equation (3), is scaled with the gyration period. The canonical momenta are mapped to velocities via $p_y = \dot{y}$, $c_4 = \dot{z} - \frac{1}{2} y^2$. I_2 is an integral of motion yielding the velocity of the x-component of motion (missing in Equation (3)), namely:

$$I_2 = \dot{x} - \xi_\parallel y + \xi_\perp z. \tag{4}$$

In addition, we found (Efthymiopoulos, Gontikakis, and Anastasiadis, 2005; Gontikakis, Efthymiopoulos, and Anastasiadis, 2006) that the maximum kinetic energy gain for one particle can be expressed as a function of the field parameters, the position of injection into the sheet and the initial energy of the particle with the relation

$$E_{\max} = \frac{\epsilon}{\xi_\perp^2}\left(\xi_\perp I_2 + \xi_\parallel \xi_\perp y_{\text{out}} + \epsilon + \sqrt{2\xi_\perp I_2 \epsilon + 2\xi_\parallel \xi_\perp y_{\text{out}}\epsilon + \epsilon^2 + 2\xi_\perp^2 E_0}\right), \quad (5)$$

where E_0 is the initial kinetic energy of a particle injected at $y = y_0$, the value of I_2 is to $I_2 = \dot{x}_0 - \xi_\parallel y_0$, and the exit of the particle is through the edge $y = y_{\text{out}}$.

The study of the particle orbits in a Harris-type current sheet, given by Equation (1), is done by integrating numerically the relevant equations of motion using the Hamiltonian of the form given in Equation (3). For the case of an X-point geometry we integrate the Newtonian equations of motion using Equation (2) for the electromagnetic field. In all our numerical simulations we consider that the RCS half-thickness a is the unit of length and the inverse gyrofrequency $\omega_B^{-1} = m/qB_0$ is the unit of time. For a typical value of the main magnetic field $B_0 = 100G$, $\omega_B^{-1} \simeq 6 \times 10^{-10}$ sec for electrons and 10^{-6} sec for protons. A super-Dreicer electric field E of 100 V m^{-1} is used, which corresponds to a normalized field of $\epsilon = 10^{-5}$ for electrons and of $\epsilon = (m_p/m_e) \times 10^{-5} \simeq 1.84 \times 10^{-2}$ for protons. The numerical integration is carried out, for both geometries, until the particle reaches the edges of the reconnection site which is at $y = \pm 1$. Finally, we consider particle injections at three different positions along the y-axis, *i.e.*, from the edges ($y = \pm 0.9$) or from the central plane ($y = 0$).

3. Particle Interactions with a Single RCS

Particles can follow several types of orbits inside reconnecting magnetic fields. The form of the orbit depends strongly on the value of the longitudinal component of the magnetic field $\xi_\parallel$. When $\xi_\parallel$ is less than about 0.1, electrons can follow chaotic orbits which lead them to escape, or regular quasi-periodic orbits along which the particle remains trapped in the sheet. In Figure 1 two kinds of electron orbits are shown inside a RCS. In the first case (panels a, b) the particle never reaches the $y = \pm 1$ edges and performs a quasi-periodic motion, mirrored by the growth of the magnetic field strength away from the $y = 0$ plane. The second orbit (panels c, d) is an escaping chaotic orbit. Initially the electron oscillates in the y-axis with $|y| < 0.05$. Later however, it leaves the current sheet by moving along a magnetic field line. For large values of $\xi_\parallel$ most particles follow adiabatic orbits. In that case the particles nearly follow adjacent magnetic field lines before escaping from the accelerating site.

Chaotic and regular (adiabatic) orbits are also found in the case of acceleration through an X-point configuration. In Figure 2 an electron moves chaotically through an X-point with $\xi_\parallel = 0$, $\xi_\perp = 10^{-3}$ and $\epsilon = 10^{-5}$. The electron starts its motion at $(x_0, y_0) = (0, 0.9)$ and, then drifts toward the X-point line at $(x, y) = (0, 0)$. There, it performs a bounce motion which pushes it to larger values of y until it reaches the $y = 1$ edge where it escapes from the current sheet.

We now consider the acceleration of $N = 30\,000$ particles (electrons or protons) that form initially a thermal distribution at a typical coronal temperature of 2×10^6 K. This means that the velocities of particles are randomly oriented and form a Maxwellian distribution. Each particle enters from one of the three selected injection points along the y-axis, namely $y = \pm 0.9$ or $y = 0$. The initial position of the particles on the x-axis is defined as $|x| < 0.5$ for X-points and $x = 0$ for Harris-type current sheets. The field parameters, for both current sheets configurations, are $\xi_\parallel = 1$, $\xi_\perp = 10^{-3}$ with dimensionless electric field parameters $\epsilon = 10^{-5}$ for electrons and $\epsilon = 1.84 \times 10^{-2}$ for protons.

In Figure 3, we present a comparison between particles accelerated through a Harris-type current sheet and particles accelerated through an X-point. The presented characteristics are the final kinetic energy distribution and the final pitch angle distribution of the particles. In

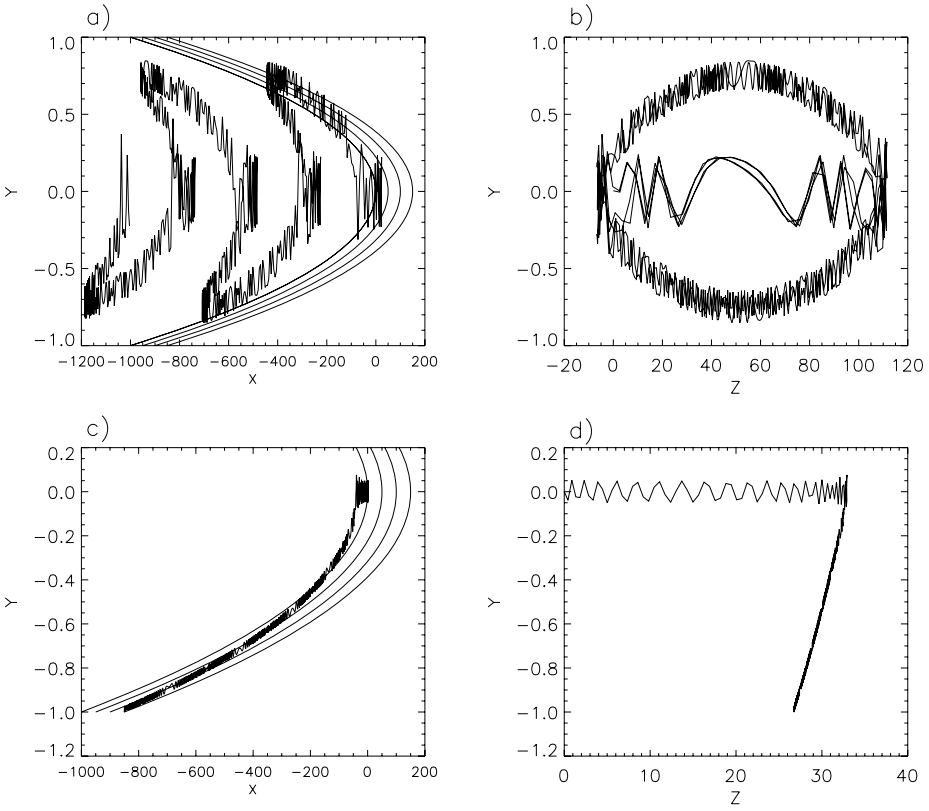

Figure 1 Examples of single electron orbits inside a Harris-type reconnecting current sheet with $\xi_{\parallel} = 0$ and $\xi_{\perp} = 10^{-3}$. In panels (a) and (b) the projections of a trapped (mirrored) trajectory are shown. In panels (c) and (d) the projections of an escape orbit are presented. The continuous lines in panels (a) and (c) are visualizations of the magnetic field lines.

all the kinetic energy distribution plots, the dotted vertical lines correspond to the maximum kinetic energy gain computed using Equation (5). Electron kinetic energy distributions have a short energy range that is characterized by a number of energy peaks. In the Harris-type case three energy peaks correspond to the initial injection positions. In the case of X-points, the distribution presents two peaks, one for particles injected from the sides ($y = \pm 0.9$) and one, with higher energy, for injection from the X-point center. Moreover, for the same parameter values used in both geometries, particles accelerated in an X-point gain less kinetic energy by a factor of $\simeq 10$. Because of the fact that the particles entry points are very localized in the y-axis, the resulting final kinetic energy distributions are peaked in a short range of final energies rather than yielding a power-law (like in Wood and Neukirch (2005); our case best compares with Figure 5 of that paper, which corresponds to particles accelerated near the separatrix). On the other hand, our injection of particles at $y = 0$ is representative of particles being accelerated when they start already inside the current sheet. In fact, if a uniform distribution of initial conditions is taken in the range $-0.9 \leq y \leq 0.9$ the final kinetic energy distribution fills the gaps between the peaks of Figure 3a, c.

The analytic formula of Equation (5) predicts well the numerical result, especially in the case of the Harris-type (Gontikakis, Anastasiadis, and Efthymiopoulos, 2007). In the

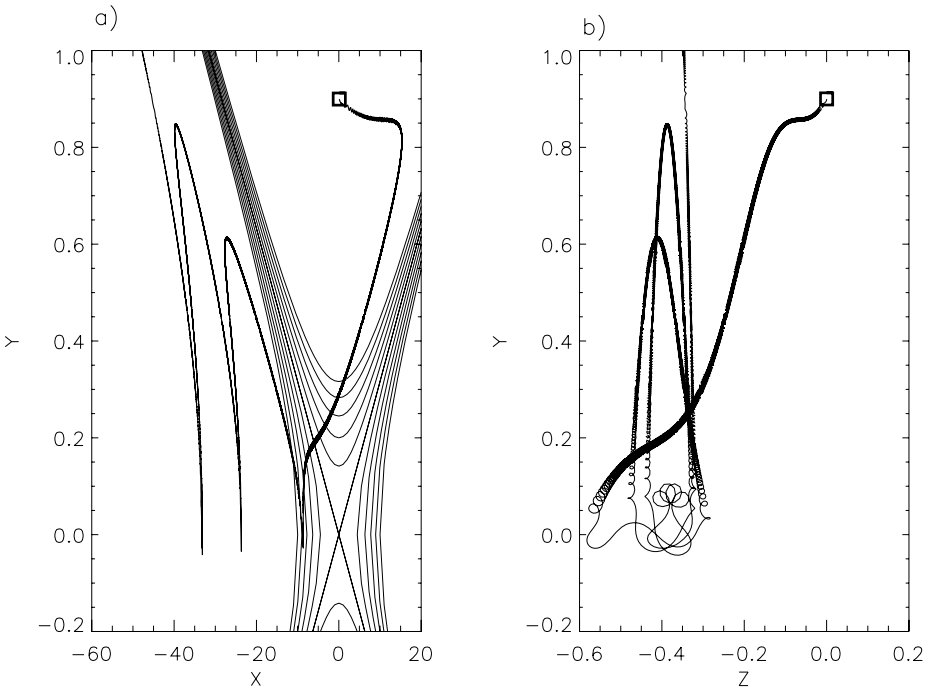

Figure 2 Example of single electron orbit inside an X-point configuration, with $\xi_{\parallel} = 0$ and $\xi_{\perp} = 10^{-3}$. The continuous lines in panel (a) are visualizations of the magnetic field lines.

case of the acceleration through the X-point on the other hand, the analytical solution gives a reasonable estimation for the particles entering from the upper edge if we replace the parameter $\xi_{\perp}$ with an effective value (see below). As the particle moves along the x-axis it encounters an increasing value of the perpendicular component of the magnetic field, $B_y = \xi_{\perp} x$. Roughly, one can replace $\xi_{\perp}$ with $\xi_{\perp}\langle x\rangle$ ($\langle x\rangle$ is the average position along the x-axis of a particle orbit) in Equation (5) which gives the right estimation of the kinetic energy gain. The analytic expression is consistent with the numerical results as long as the particles enter from the sides of the X-point and is slightly short in energy for electrons starting at the X-point center (panel c). In fact, as already mentioned, in the adiabatic limit the projection of the orbits of the particles on the $x-y$ plane follows essentially the projection of the magnetic field lines on the same plane. The latter is given by the family of hyperbolas:

$$y^2 - \xi_{\perp} x^2 = \text{const.} \tag{6}$$

Particles entering the sheet at (x_0, y_0) and leaving the sheet at $(x_{\text{out}}, y_{\text{out}})$ then satisfy approximately the relation $|x_{\text{out}}| \simeq (1/\sqrt{\xi_{\perp}})\sqrt{y_{\text{out}}^2 - y_0^2 - \xi_{\perp} x_0^2}$. The average transverse magnetic field 'felt' by the particles can then be estimated as

$$\langle \xi_{\perp} \rangle \approx \frac{\xi_{\perp}}{2}\left(\left(1/\sqrt{\xi_{\perp}}\right)\sqrt{y_{\text{out}}^2 - y_0^2 - \xi_{\perp} x_0^2} - x_0 \right). \tag{7}$$

Then, Equation (5) can be used to estimate analytically the maximum amount of kinetic energy gain for the particles crossing an X-point if $\xi_{\perp}$ in Equation (5) is substituted for $\langle \xi_{\perp} \rangle$ from Equation (7).

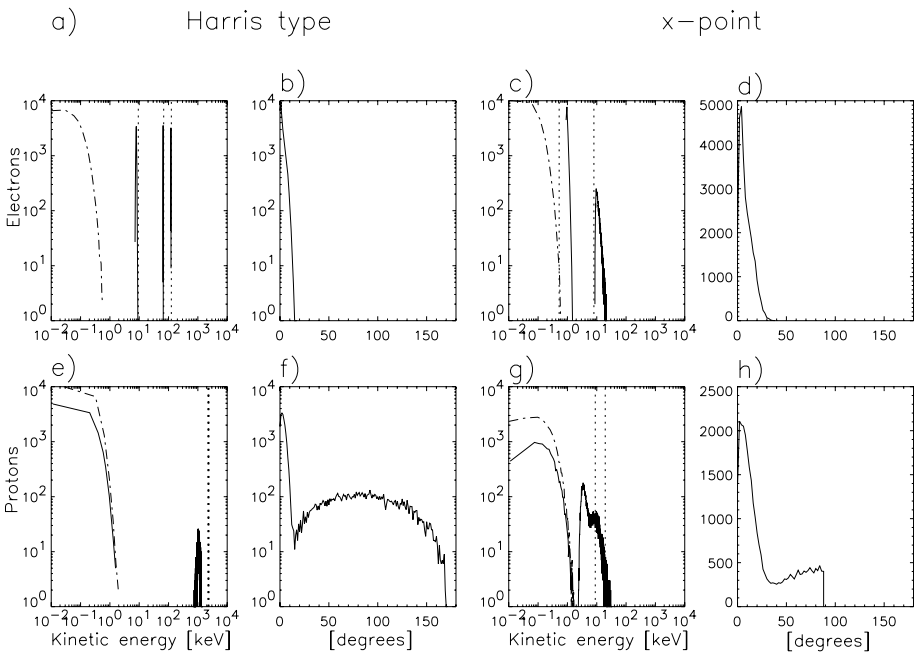

Figure 3 Distributions of kinetic energy and pitch angles for a Harris-type (panels a, b, e and f) and an X-point (panels c, d, g and h) RCS with $\xi_{\parallel} = 1$ and $\xi_{\perp} = 10^{-3}$. (a), (b), (c), and (d) correspond to electrons and (e), (f), (g), and (h) to protons. In panels (a), (c), (e) and (g) the dashed-dotted line corresponds to the initially injected kinetic energy distribution and the vertical dotted lines to maximum kinetic energy derived by the analytical formula given by Equation (5).

Protons present a behavior which is quite common in both the Harris-type and X-point types of accelerators. In particular, a large fraction of the initially injected protons are not accelerated, but they simply cross the current sheet practically without changing their kinetic energy. The final kinetic energy distribution of these protons is thus still a Maxwellian (see Figure 3 panels e and g). On the other hand, as in the case of electrons, the kinetic energy distributions of accelerated protons present secondary features also due to the three different positions of injection. Nevertheless, such features are less apparent because the overall distribution is broader for protons than for electrons. In the case of an X-point, the kinetic energy distribution of the accelerated protons presents two components, one associated with an injection from the sides and the other with an injection from the center of the current sheet.

In a Harris-type, the final kinetic energy of protons is of the order of 1 MeV, which is 10 times larger than the energy gain of electrons. In the case of an X-point, protons and electrons are both seen to gain considerably less energy, of the order of 10 keV. As regards exit pitch angle distributions, both electrons and protons, accelerated in either X-point or Harris-type current sheets, present similar narrow distributions (Figure 3b, d, f, h). The pitch angle distributions of protons exhibit a broad band corresponding to the population of non-accelerated particles, the velocities of which are randomly oriented both before and after the interaction with the RCS.

Finally, we studied the time needed for a particle to leave a current sheet as a function of the longitudinal magnetic field component $\xi_{\parallel}$. The time needed for an electron to leave the current sheet is of the order or a few microseconds. For protons the time is of some

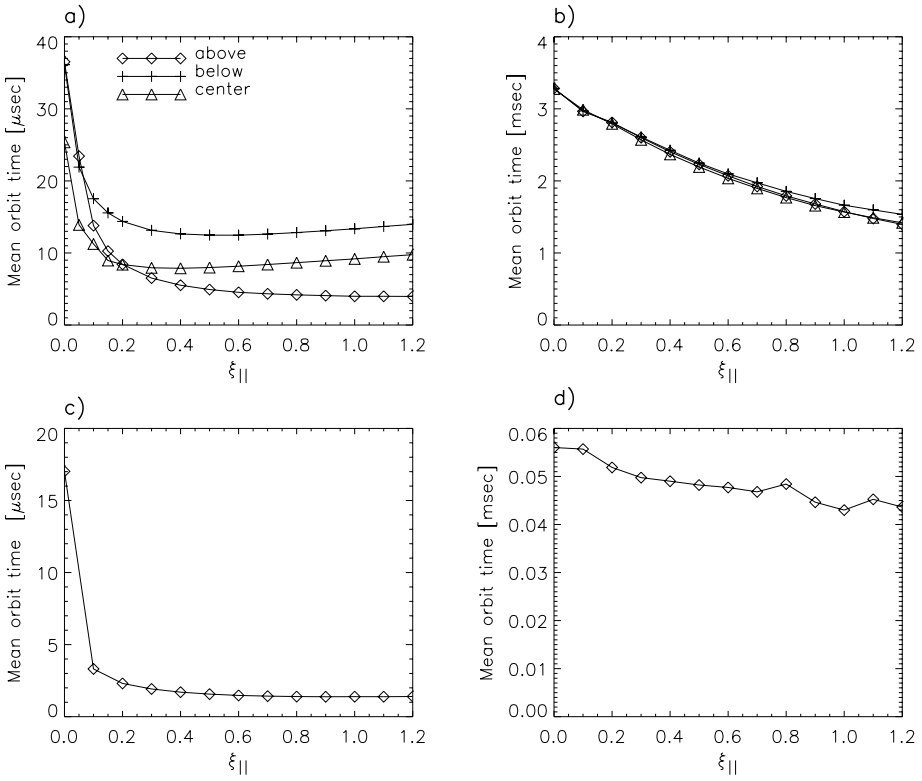

Figure 4 Time spent by accelerated particles inside ($|y| < 1$) a current sheet depending on the value of the $\xi_\parallel$ with $\xi_\perp = 10^{-3}$. (a) and (b) correspond to a Harris-type while (c) and (d) to an X-point RCS, respectively. In panels (a) and (c) the particles are electrons and in panels (b) and (d) protons. In (a) and (b), diamonds shows injections from above, crosses injections from below and triangles from the center of the current sheet. Particles are injected from the sides of X-points. The electric field is of 10^{-5} and 1.84×10^{-2} for electrons and protons, respectively.

milliseconds (Gontikakis, Anastasiadis, and Efthymiopoulos, 2007). Note that such time scales are still out of the time resolution of present instruments, thus little can be said as regards comparison of those values with observations. In order to compute the mean time needed for the particles to reach the edges of current sheets (at $y = \pm 1$), we followed the orbits of 1000 protons and electrons through a Harris-type and an X-point current sheet for values of the $\xi_\parallel$ in the range (0 to 1.2). In Figure 4 we present the mean time as a function of the value of $\xi_\parallel$ for electrons (panel a) and protons (panel b). For protons, the time inside the current sheet is a decreasing function of $\xi_\parallel$. For electrons, the acceleration time decreases sharply when $\xi_\parallel$ changes from 0 to 0.1. This function also depends on the injection point. Electrons entering the current sheet from above have acceleration times slowly decreasing with $\xi_\parallel$. On the other hand, electrons starting from the center or entering from below ($y = -0.9$) show a small rise of the acceleration time as a function of $\xi_\parallel$. In the case of electrons, when $y_0 \neq 0.9$ the acceleration time grows asymptotically, for large $\xi_\parallel$, as a function of $\xi_\parallel$. This result is in agreement with the asymptotic analysis of Litvinenko (1996) in the case of strongly magnetized particles.

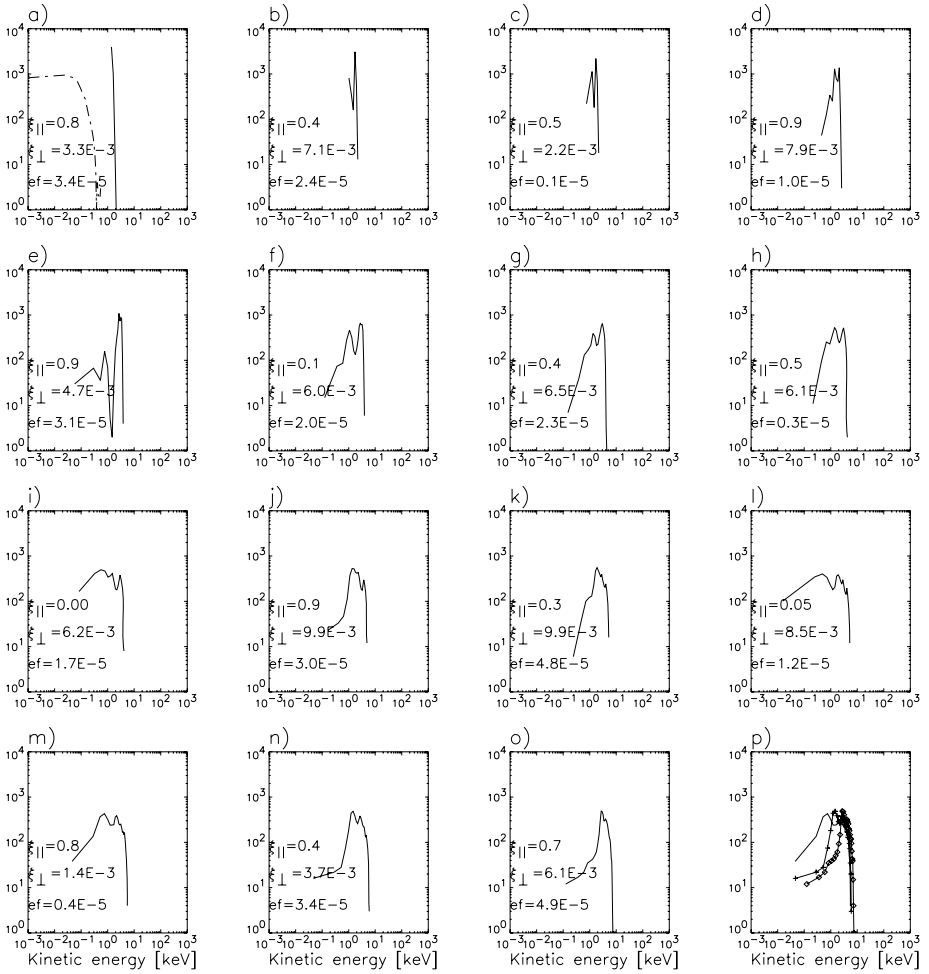

Figure 5 Consecutive acceleration of 5000 electrons, initially with thermal velocities, in 15 X-points. Each panel from left to right and from top to bottom shows the final kinetic energy distribution of the electrons after the interaction with each X-point. In the first panel, the dashed-dotted curve is the initial thermal kinetic energy distribution. Panel (p) shows the three last distributions.

4. Particle Interactions with Multiple RCSs

As already stated in the Introduction, an appropriate description of the environment within which the particle acceleration takes place involves considering the coexistence of multiple reconnecting current sheets. In this section, we present our numerical results for the interaction of electrons and protons with multiple current sheets taking random parameter values from a homogeneous distribution, together with a theoretical analysis of these results.

4.1. Numerical Results

We performed numerical simulations of particles interaction successively with 15 current sheets. In a previous work (Gontikakis, Anastasiadis, and Efthymiopoulos, 2007) we stud-

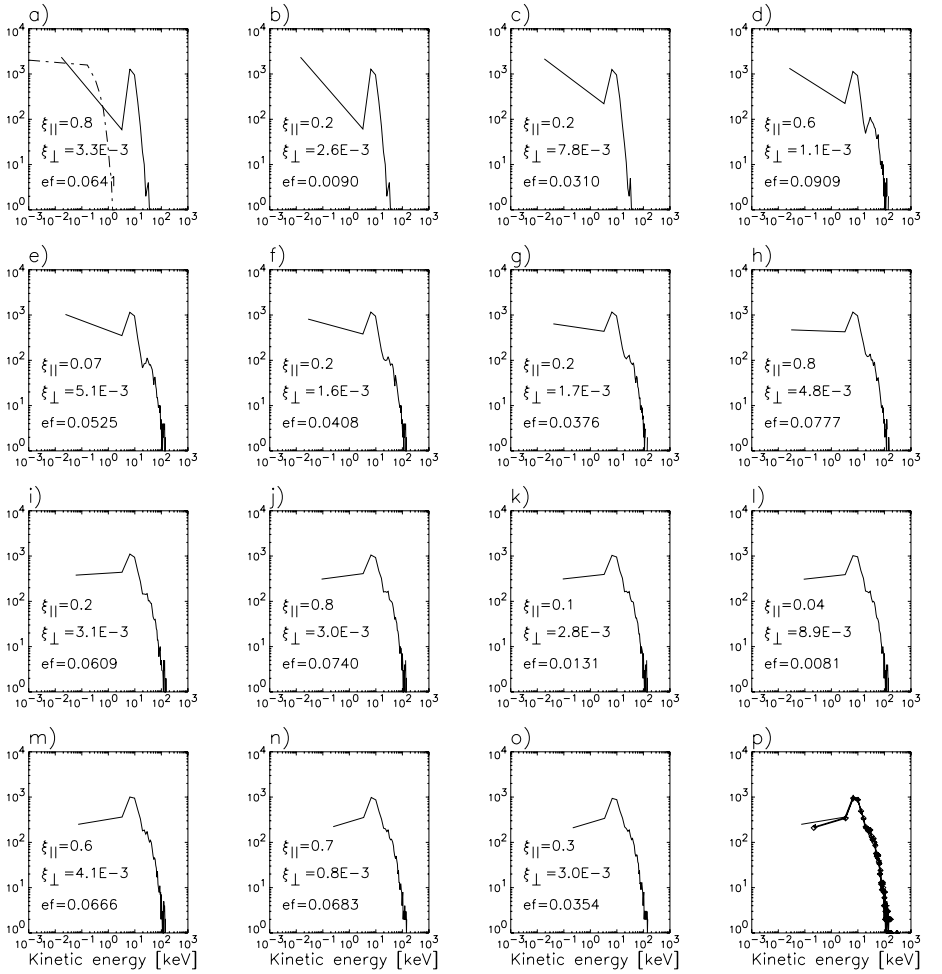

Figure 6 Same as for Figure 5 for protons.

ied the cases of electrons and protons accelerated successively in Harris-type current sheets. In the present work we present the acceleration of protons and electrons in X-point reconnecting current sheets. We consider 5000 particles that have initially a thermal kinetic energy at 2×10^6 K. They are injected in the first X-point of the series. The injection points of the particles are at $y = \pm 0.9$ and their initial positions along the x-axis vary randomly inside the range $-0.5 < x < 0.5$. The particles with modified kinetic energies after the interaction with the first X-point are injected through the next RCS. This procedure is repeated 15 times. The parameters $\xi_\parallel$ and $\xi_\perp$ for each RCS are selected randomly in the range: $10^{-4} < \xi_\perp < 10^{-2}$, $0.01 < \xi_\parallel < 1$. Similarly the normalized electric field is randomly selected in the range $10^{-6} < \epsilon < 5 \times 10^{-5}$ for electrons and $1.84 \times 10^{-3} < \epsilon < 9.2 \times 10^{-2}$ for protons. The orientations of the velocities of accelerated particles are randomized every time before their injection into the next current sheet.

The resulting distributions are presented in Figure 5 for electrons and in Figure 6 for protons. The main result found again is that the evolution of the kinetic energy distribution

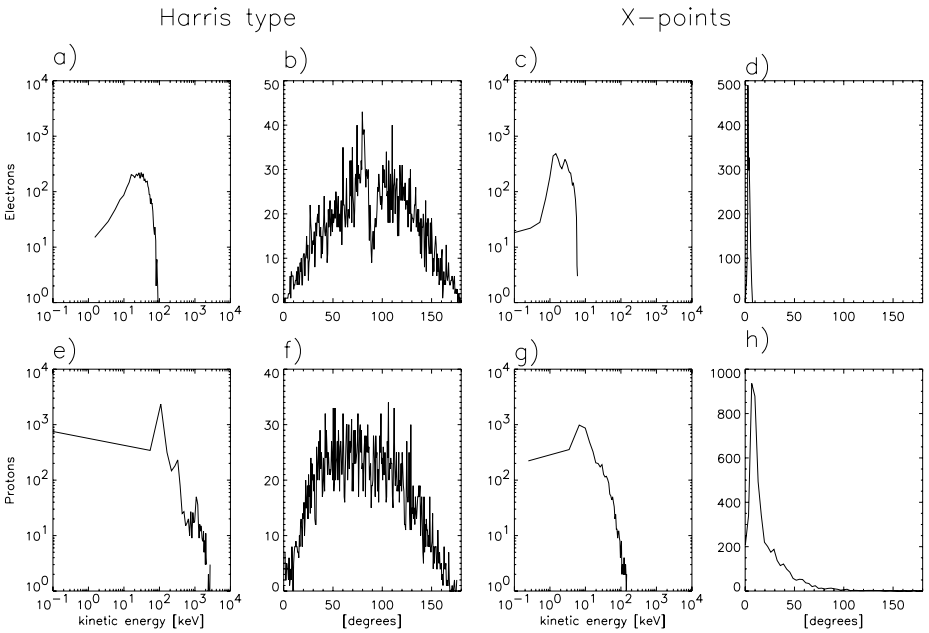

Figure 7 Distributions of kinetic energy and pitch angle for multiple encounters of protons and electrons with Harris-type (panels a, b, e and f) and X-point (panels c, d, g and h) current sheets. (a), (b), (c), and (d) correspond to electrons and (e), (f), (g), and (h) to protons. Panels a, c, e, g show the final kinetic energy of the particles whereas panels b, d, f, h the final pitch angle distributions.

converges towards a final state after a small number of current sheets encounters. This happens for both types of particles and in both types of current sheet configurations. In panel (p) of Figures 5 and 6 one can compare the last three kinetic energy distributions (13th, 14th and 15th) and conclude that they have the same shape at high energies. The same result was also found for the case of multiple encounters with Harris-type current sheets (see Gontikakis, Anastasiadis, and Efthymiopoulos, 2007).

For the case of X-points, the maximum kinetic energy gain is of the order of 10 keV for electrons and of 100 keV for protons. In Figure 7 one can compare the final kinetic energy distributions for multiple encounters with Harris-type (panels a, e) and X-point (panels c, g) RCSs. As was the case for single encounters, particles interacting with Harris-type RCS gain more energy, in a factor of 10, than when they interact with X-point current sheet configurations.

4.2. Theoretical Analysis

In Gontikakis, Anastasiadis, and Efthymiopoulos (2007) a heuristic explanation was given for the asymptotic convergence of the kinetic energy distribution in a multiple particle-RCS interaction. The explanation was that as the input kinetic energy increases, the probability of an RCS, with random parameters $(\xi_\perp, \xi_\parallel, \epsilon)$ within a specified parameter space, to be an efficient accelerator decreases. We hereby provide a detailed theoretical treatment of these results.

Let w_0 be the maximum percentage of kinetic energy gain for particles with initial energy E_0 interacting with a Harris-type RCS with parameters $(\xi_\perp, \xi_\parallel, \epsilon)$. We consider in detail

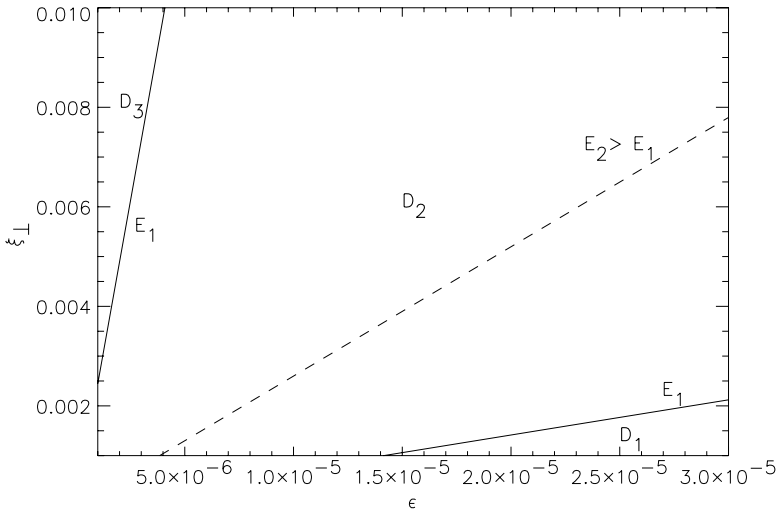

Figure 8 The full domain range $10^{-6} \leq \epsilon \leq 3 \times 10^{-5}$, $10^{-3} \leq \xi_\perp \leq 10^{-2}$. The lower and upper solid lines are the graphs of Equations (12) and (13), respectively for $w_0 = 1$, $E_0 = E_1 = 4.7$ keV. A kinetic energy gain $w_0 E_1$ is possible for all values of $\xi_\parallel$ in the domain D_1 and for some values of $\xi_\parallel$ in the domain D_2, while it is not possible in the domain D_3. The dashed line is the graph of Equation (13) for $w_0 = 1$ and $E_0 = E_2 = 47$ keV.

the case of particles entering the RCS at $z = 0$ with $\dot{x}_0 = 0$. Thus, $I_2 = -\xi_\parallel y_0$. Setting $E_{\max} = w_0 E_0$ in Equation (5) yields

$$\xi_\perp \xi_\parallel \Delta y + \epsilon + \sqrt{2\epsilon \xi_\perp \xi_\parallel \Delta y + \epsilon^2 + 2\xi_\perp^2 E_0} = \frac{w_0 \xi_\perp^2 E_0}{2}, \tag{8}$$

where $\Delta y = y_{\text{out}} - y_0$. Equation (8) can be used in order to find the critical value of $\xi_\parallel$ above which the kinetic energy gain surpasses the percentage w_0 for fixed values of the remaining parameters. Setting $\xi_\parallel = 0$ in Equation (8) yields the minimum percentage

$$w_{\text{m}} = \frac{\epsilon}{\xi_\perp^2 E_0} \left(\epsilon + \sqrt{\epsilon^2 + 2\xi_\perp^2 E_0} \right). \tag{9}$$

If $w_0 > w_{\text{m}}$ Equation (8) admits a positive solution for $\xi_\parallel$ provided that

$$\xi_\parallel \leq \frac{w \xi_\perp E_0}{\epsilon \Delta y} - \frac{\epsilon}{\xi_\perp \Delta y}. \tag{10}$$

The solution reads

$$\xi_\parallel = \frac{1}{\Delta y} \left[\frac{w_0 \xi_\perp E_0}{\epsilon} - \sqrt{2(w_0 + 1) E_0} \right]. \tag{11}$$

If $\xi_\parallel$ is greater than the value given by Equation (11), the percentage of kinetic energy gain is larger than w_0. We now estimate, for fixed (w_0, E_0) the probability within the parameter space that an RCS accelerates the particles by a percentage larger or equal than w_0. This can be done with the help of Figure 8. This figure shows the domain of the parameter space for ϵ and $\xi_\perp$, which in our simulations is $10^{-6} \leq \epsilon \leq 3 \times 10^{-5}$, $10^{-3} \leq \xi_\perp \leq 10^{-2}$. The lower

solid line corresponds to the equation

$$\xi_\perp = \frac{\epsilon}{w_0}\sqrt{\frac{2(w_0+1)}{E_0}}. \tag{12}$$

This line corresponds to the locus of values $(\epsilon, \xi_\perp)$ for which the given percentage w_0 coincides with the minimum possible percentage of kinetic energy gain for the given energy E_0, according to Equation (9). This line divides the full domain in two domains. In the lower domain (D_1) one has $w_\mathrm{m} > w_0$, thus for all values of $\xi_\parallel$ the kinetic energy gain is higher than w_0. On the other hand, in the upper domains (D_2 and D_3) one has $w_\mathrm{m} < w_0$, thus only for $\xi_\parallel$ large enough the percentage w_0 can be surpassed. Now, the upper solid line corresponds to the locus where the minimum value of $\xi_\parallel$, for which the percentage w_0 is reached, exceeds the upper allowed value $\xi_{\parallel,\max}$ within the selected parameter space (in our examples $\xi_{\parallel,\max} = 1$). This is given by

$$\xi_\perp = \frac{\epsilon}{w_0}\left(\sqrt{\frac{2(w_0+1)}{E_0}} + \frac{\Delta y}{w_0 E_0}\right). \tag{13}$$

In the domain D_3, above the line given by Equation (13), we have $\xi_\parallel > \xi_{\parallel,\max}$, thus this domain lies entirely outside the parameter space. In view of the above analysis, the total subvolume of the parameter space in which the kinetic energy gain exceeds the percentage w_0 is given by

$$V(w_0, E_0) = (\xi_{\parallel,\max} - \xi_{\parallel,\min})S(D_1) + \int_{D_2} \left(\xi_{\parallel,\max} - \xi_\parallel(w_0, E_0, \xi_\perp, \epsilon)\right) \mathrm{d}\xi_\perp \, \mathrm{d}\epsilon, \tag{14}$$

where $\xi_{\parallel,\max}$ and $\xi_{\parallel,\min}$ are the limits of $\xi_\parallel$ in the selected parameter space, $S(D_1)$ is the surface of the domain D_1 and $\xi_\parallel(w_0, E_0, \xi_\perp, \epsilon)$ is the solution for $\xi_\parallel$ (see Equation (11)). The probability of an RCS to accelerate the particles in a gain factor larger than w_0 is given by

$$P(w_0, E_0) = \frac{V(w_0, E_0)}{V_\mathrm{total}}. \tag{15}$$

This probability is roughly proportional to the total area of the domains D_1 and D_2 over the full domain area. We can see now that as E_0 increases, the probability $P(w_0, E_0)$ decreases for any fixed value of w_0. This is simply because, according to Equations (12) and (13) the slopes of both limiting lines decrease, thus the total area $S(D_1) + S(D_2)$ also decreases. In fact, beyond a sufficiently high value of E_0, at which the upper limiting line touches the lower right boundary of the full domain, domains D_1 and D_2 have null areas. Thus, the probability of a gain factor w_0 shrinks to zero. This was precisely found numerically in Figure 9 of Gontikakis, Anastasiadis, and Efthymiopoulos (2007) (note an error in this figure: w there corresponds to $w_0 - 1$ in our notation). Setting the value $w_0 = 1$ (corresponding to $w = 0$ in Gontikakis, Anastasiadis, and Efthymiopoulos, 2007), as well as $\xi_\perp = 10^{-3}$ and $\epsilon = 3 \times 10^{-5}$ for the lower right boundary of the full domain and $\xi_{\parallel,\max} = 1$, we find a maximum energy using Equation (8) equal to $E_0 \simeq 7.5 \times 10^{-2}$, or, in physical units $E_0 = 4.2 \times 10^2$ keV, which agrees well with the limit found numerically in Gontikakis, Anastasiadis, and Efthymiopoulos (2007).

5. Conclusions

In the present work we studied the acceleration of electrons and protons in a multiple particle-RCS interaction scenario, assuming two different reconnection topologies, the Harris-type and X-point current sheets. Our main conclusions are the following:

1. The particles accelerated close to an X-point, with specific field parameters $(\xi_\perp, \xi_\parallel, \epsilon)$ gain a smaller amount of kinetic energy than particles accelerated through a Harris-type current sheet with the same model parameters. This is because particles accelerated through an X-point encounter a stronger average perpendicular magnetic field component.
2. The particles escape from a Harris-type current sheet in longer times than from an X-point current sheet.
3. A previously derived analytical formula (Equation (5)), yielding the maximum kinetic energy gain for particles accelerated through a Harris-type topology (Gontikakis, Efthymiopoulos, and Anastasiadis, 2006), provides a satisfactory approximation to the kinetic energy gains computed numerically. Equation (5) can also be modified to yield an estimate for the kinetic energy gain of particles accelerated in an X-point if the perpendicular component $\xi_\perp$ is replaced by an effective field $\langle \xi_\perp \rangle$, which is the mean perpendicular magnetic field along an orbit.
4. A number of similarities are also found for the acceleration of particles through Harris-type and X-point RCSs. An important fraction of protons with initially thermal distributions are not accelerated at all. The pitch angle distributions of the accelerated electrons and protons present sharp peaks for angles $< 10°$.
5. When the particles encounter multiple RCSs with parameters obtained randomly from a uniform sample, the particle kinetic energy distribution tends to acquire a limiting form after some iterations. This tendency was previously observed (Gontikakis, Anastasiadis, and Efthymiopoulos, 2007) in the case of multiple encounters with Harris-type RCSs, and we here confirm it also in the case of X-points. A theoretical explanation is given by considering the probability of an RCS to act as efficient accelerator (parametrized by the percentage w_0 of kinetic energy gain with respect to some initial energy E_0). In particular, we demonstrate analytically that this probability decreases as E_0 increases.

Acknowledgements We wish to thank Dr. I. Contopoulos for stimulating discussions on the problem of magnetic reconnection, as well as the anonymous referee, and Dr. K-L. Klein for their comments and suggestions that improved our manuscript. The work of C.G. and C.E. was supported in part by the Research Committee of the Academy of Athens. A.A. would like to thank the members of the Particle Acceleration Working Group of the CESRA-2007 workshop for many stimulating discussions.

References

Anastasiadis, A.: 2002, *J. Atmos. Solar Terr. Phys.* **64**, 481.
Anastasiadis, A., Vlahos, L.: 1991, *Astron. Astrophys.* **245**, 271.
Anastasiadis, A., Vlahos, L.: 1994, *Astrophys. J.* **428**, 819.
Anastasiadis, A., Vlahos, L., Georgoulis, M.K.: 1997, *Astrophys. J.* **489**, 367.
Anastasiadis, A., Gontikakis, C., Vilmer, N., Vlahos, L.: 2004, *Astron. Astrophys.* **422**, 323.
Aschwanden, M.J., Montello, M., Dennis, B.R., Benz, A.O.: 1995, *Astrophys. J.* **440**, 394.
Aschwanden, M.J., Tarbell, T.D., Nightingale, R.W., Schrijver, C.J., Title, A., Kankelborg, C.C., Martens, P., Warren, H.P.: 2000, *Astrophys. J.* **535**, 1047.
Benz, A.O.: 1985, *Solar Phys.* **96**, 357.
Benz, A.O., Kosugi, T., Aschwanden, M.J., Benka, S.G., Chupp, E.L., Enome, S., Garcia, H., Holman, G.D., Kurt, V.G., Sakao, T.: 1994, *Solar Phys.* **153**, 33.

Browning, P.K., Vekstein, G.E.: 2001, *J. Geophys. Res.* **106**, 18677.
Bruhwiler, D.L., Zweibel, E.G.: 1992, *J. Geophys. Res.* **97**, 10825.
Bulanov, S.V.: 1980, *Sov. Astron. Lett.* **6**, 206.
Burkhart, G.R., Drake, J.F., Chen, J.: 1990, *J. Geophys. Res.* **95**, 18833.
Craig, I.J.D., Litvinenko, Y.E.: 2002, *Astrophys. J.* **570**, 387.
Crosby, N.B., Aschwanden, M.J., Dennis, R.B.: 1993, *Solar Phys.* **143**, 275.
Crosby, N.B., Vilmer, N., Lund, N., Sunyaev, R.: 1998, *Astron. Astrophys.* **334**, 299.
Dalla, S., Browning, P.K.: 2005, *Astron. Astrophys.* **436**, 1103.
Dauphin, C., Vilmer, N., Anastasiadis, A.: 2007, *Astron. Astrophys.* **468**, 273.
Deeg, H.J., Borovsky, J.E., Duric, N.: 1991, *Phys. Fluids B* **3**, 2660.
Dennis, B.R.: 1985, *Solar Phys.* **100**, 465.
Efthymiopoulos, C., Gontikakis, C., Anastasiadis, A.: 2005, *Astron. Astrophys.* **443**, 663.
Fletcher, L., Petkaki, P.: 1997, *Solar Phys.* **172**, 267.
Gontikakis, C., Efthymiopoulos, C., Anastasiadis, A.: 2006, *Mon. Not. Roy. Astron. Soc.* **368**, 293.
Gontikakis, C., Anastasiadis, A., Efthymiopoulos, C.: 2007, *Mon. Not. Roy. Astron. Soc.* **378**, 1019.
Hamilton, B., McClements, K.G., Fletcher, L., Thyagaraja, A.: 2003, *Solar Phys.* **214**, 339.
Hamilton, B., Fletcher, L., McClements, K.G., Thyagaraja, A.: 2005, *Astrophys. J.* **625**, 496.
Hannah, I.G., Fletcher, L.: 2006, *Solar Phys.* **236**, 59.
Heerikhuisen, J., Litvinenko, Y.E., Craig, I.J.D.: 2002, *Astrophys. J.* **566**, 512.
Hughes, D., Paczuski, M., Dendy, R.O., Helander, P., McClements, K.G.: 2003, *Phys. Rev. Let.* **90**(13), 131101.
Isliker, H., Anastasiadis, A., Vlahos, L.: 2001, *Astron. Astrophys.* **377**, 1068.
Kliem, B.: 1994, *Astrophys. J. Suppl.* **90**, 719.
Krucker, S., Benz, A.O.: 1998, *Astrophys. J.* **501**, L213.
Litvinenko, Y.E.: 1996, *Astrophys. J.* **462**, 997.
Litvinenko, Y.E., Somov, B.: 1993, *Solar Phys.* **146**, 127.
Martens, P.: 1988, *Astrophys. J.* **330**, 131.
Martens, P., Young, A.: 1990, *Astron. Astrophys. Suppl.* **73**, 333.
Mercier, C., Trottet, G.: 1997, *Astrophys. J.* **474**, L65.
Miller, J.A., Cargill, P.J., Emslie, A.G., Holman, G.D., Dennis, B.R., LaRosa, T.N., Winglee, R.M., Benka, S.G., Tsuneta, S.: 1997, *J. Geophys. Res.* **102**, 14631.
Mori, K.I., Sakai, J.I., Zhao, J.: 1998, *Astrophys. J.* **494**, 430.
Moses, R.W., Finn, J.M., Ling, K.M.: 1993, *J. Geophys. Res.* **98**, 4013.
Onofri, M., Isliker, H., Vlahos, L.: 2006, *Phys. Rev. Let.* **96**, 1102.
Parker, E.N.: 1988, *Astrophys. J.* **330**, 474.
Petkaki, P., MacKinnon, A.L.: 1997, *Solar Phys.* **172**, 279.
Petkaki, P., MacKinnon, A.L.: 2007, *Astron. Astrophys.* **472**, 623.
Saint-Hilaire, P., Benz, A.O.: 2002, *Solar Phys.* **210**, 287.
Speiser, T.W.: 1965, *J. Geophys. Res.* **70**, 4219.
Tajima, T., Sakai, J., Nakajima, H., Kosugi, T., Brunel, F., Kundu, M.R.: 1987, *Astrophys. J.* **321**, 1031.
Vekstein, G.E., Browning, P.K.: 1997, *Phys. Plasmas* **4**, 2261.
Vlahos, L., Isliker, H., Lepreti, F.: 2004, *Astrophys. J.* **608**, 540.
Wood, P., Neukirch, T.: 2005, *Solar Phys.* **226**, 73.
Zharkova, V., Gordovskyy, M.: 2004, *Astrophys. J.* **604**, 884.
Zharkova, V., Gordovskyy, M.: 2005, *Mon. Not. Roy. Astron. Soc.* **356**, 1107.